

Yield Optimization for One Pot Synthesis of Cu, Mn based Metalloporphyrin

¹Saad Nadeem*, ¹Fahim Uddin, ²Maizatul Shima Shaharun, ³Mohamed Ibrahim Abdul Mutalib

¹Chemical Engineering Department, NED University of Engineering & Technology 75300, Karachi, Pakistan.

²Department of Fundamental and Applied Sciences, Universiti Teknologi PETRONAS 32610 Bandar Seri Iskandar, Perak, Malaysia

³Department of Chemical Engineering, Universiti Teknologi PETRONAS 32610 Bandar Seri Iskandar, Perak, Malaysia.
engrsaadi61@gmail.com *

(Received on 3rd May 2021, accepted in revised form 20th January 2022)

Summary: Cu and Mn based tetraphenyl porphyrin namely CuTPP and MnTPP were synthesized through a one pot route with a modified procedure and the reaction conditions (Temperature and time) were optimized based on the energy consumption during the synthesis of the target macrocyclic ligands. The temperature (145°C and 160°C) and time (3, 4, 8 hr) were used to study the effect on the product yield. The optimized values obtained using MATLAB routines are 3.7 hr and 145°C.

Keywords: Metalloporphyrins; Optimization; Yield; Energy; Macrocycle.

Introduction

The metalloporphyrins have been studied owing to their notable traits in nearly each region of the research, from medicines to catalysis, photochemical applications and bio-sensing gadgets. Co, Fe, Mg, and Ni incorporated metalloporphyrins are the very primary metabolites and without them life might not be possible [1]. Metalloporphyrins have been significantly researched and implemented as primary materials for optical and bio sensing, photoionization processes and data storage as well [2].

Metalloporphyrins find their applicability in separation, photonic devices, magnets and sub-atomic detecting and heterogeneous catalysis. They have a remarkable propensity to specifically oxidize cyclohexane to alcohols or ketones under mild conditions with no yield of by-product. Anchoring these MePs over the inorganic frameworks improves the synergistic effects of catalyst activity and selectivity [3]. Cobalt, rhodium, and zinc based porphyrin have also been studied for free radical polymerization [4].

The field of Photodynamic treatment, Bio imaging and fluoro-immuno-tests has been investigated with the assistance of metal porphyrin edifices at close to infrared (NIR) locale [5]. Photodynamic treatment uses photosensitized charge transition from porphyrin macrocycles to the adjoining disintegrated oxygen molecules through visible light activity [6].

The solar powered water partitioning for generation of hydrogen with CO₂ reduction have additionally been considered using metalloporphyrins. The hydrogen from this procedure is an important source and can be utilized in consuming as a green and climate friendly fuel. Just like photosynthesis in the photoredox conditions the metalloporphyrins receive the light energy in the form of photons, in view of the light reaping characteristic and afterward electron generation in excited state. The electrons generated by the excited state transits to the surface of the metal counterpart (impregnated with the porphyrin moiety) for hydrogen production through water splitting and reduction of CO₂ to methanol or other liquid fuels. There is a stringent requirement of a sacrificial electron donor during this process to supplant the lost electrons by the porphyrin ligand [7, 8]. Mn (II) and Cu (II) metals with ionic radii 70 pm and 73 pm separately take an appropriate place inside the porphyrin ligand cavity to give co-planar metalloporphyrins. The D_{2h} symmetry of the free base porphyrin converts to D_{4h} during the process of metalation [9].

The current work emphasize on successful synthesis of Cu and Mn based MePs utilizing one pot synthesis route [10] with alterations [11], and optimization of their yields with respect to temperature and time based on the energy consumption during synthesis so that a large scale production could be sought afterwards. Though other types of synthesis procedures have also been reported

*To whom all correspondence should be addressed.

like for Corrole metalation with Cu, Ag and Mn [12], porphycenes with their incorporation inside mesoporous silica nanoparticles has been investigated [13] and 5,10,15,20-tetraaryl-5,15-diazaporphyrin - Tertiary amine conjugates synthesis and their electronic properties have also been discussed [14]. One pot synthesized MnTPP have also been embedded with graphene oxide for water splitting [15]. This paper is focused on the meso substituted porphyrins with Cu and Mn as the center which best suits the one pot synthesis approach as previously discussed [11].

Experimental

The chemicals were used as received for the current study are Pyrrole (97% v/v Merck Millipore), Di-methyl Formamide (98% v/v Merck), Methanol (99.999%, Merck Millipore), $\text{MnCl}_2 \cdot 4\text{H}_2\text{O}$ (99.99% w/w sigma-aldrich), $\text{CuCl}_2 \cdot 2\text{H}_2\text{O}$ (99.99% w/w sigma-aldrich), HCl (37% v/v Merck), TLC plates Silica (Sigma-Aldrich), N_2 gas (5.0) (linde HIQ), benzaldehyde (97% v/v Merck Millipore), Dichloromethane (99% v/v R&M chemicals), γ -Alumina 45 micron (99% w/w Sigma-Aldrich).

Cu/Mn centred Tetraphenyl Porphyrin synthesis (MeP, M=Mn,Cu)

Synthesis of the MeP's involves aldol condensation with a neutral solvent. The procedure is done via modification of one pot synthesis [10] as given in

with optimization for maximum yield. Benzaldehyde was used in excess. Freshly distilled Pyrrole used each time using vacuum rotary evaporator for removal of oxidized reactant and dimers. Nitrogen blanketing for the initial mixing of the reactants was employed with varying reaction temperatures (145°C and 160°C) with varying reaction duration i.e. 3, 4 and 8 hr [16] for maximum yield. Benzaldehyde and freshly distilled pyrrole in equimolar ratios mixed with HCl (catalyst) in N, N-dimethyl-formamide under nitrogen blanketing for one hour [11]. It was then refluxed using an oil bath at 145°C and 160°C for different time durations i.e., 3, 4 and 8 hours respectively.

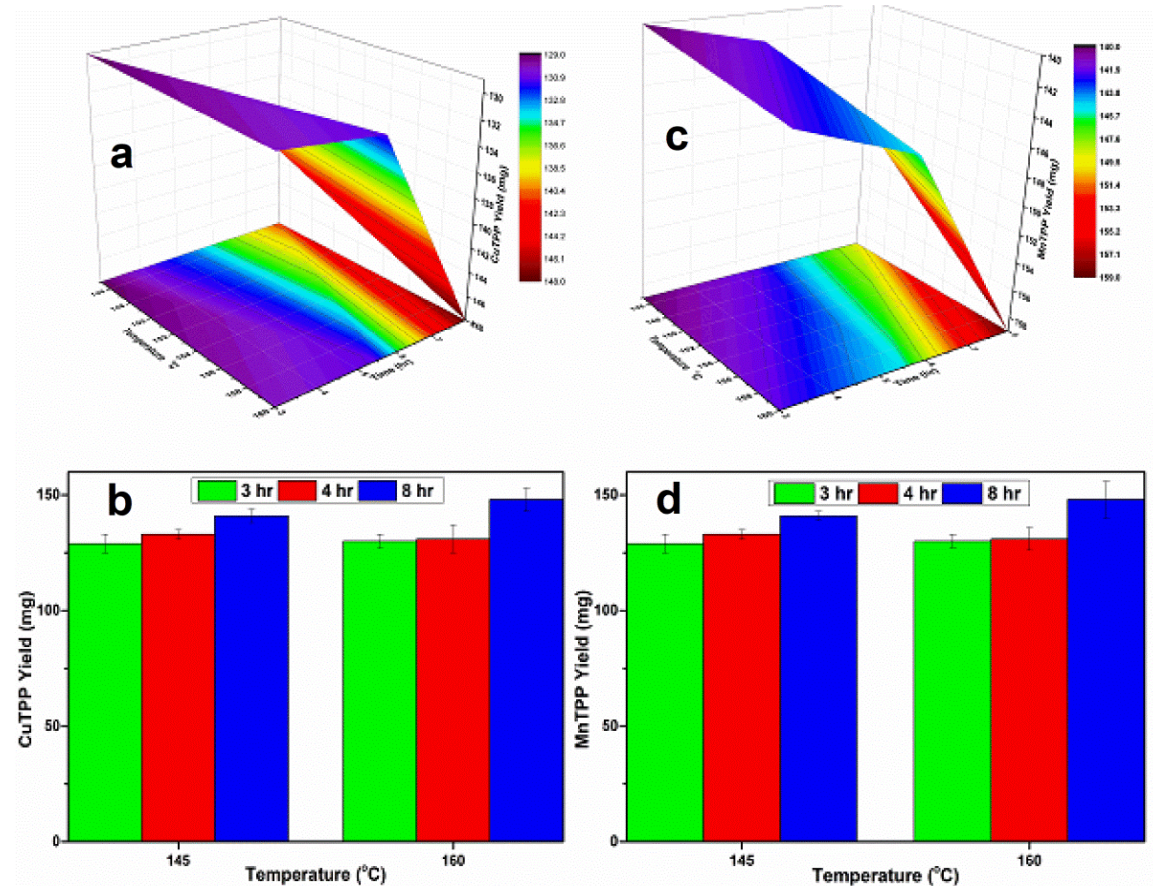


Fig. 1: Surface contours (a) CuTPP, (c) and MnTPP and yield graphs (b) CuTPP, (d) MnTPP respectively.

Purple catalyst crystals after cooling were removed via vacuum filtration followed by washing with 50 ml DMF, methanol and hot DI water three times each. The obtained crystals dried in an oven at 110°C for 12 hours with vacuum drying for 4 hrs. Dichloromethane was used to dissolve the solids after drying and purified over alumina column and analysed via TLC for purity. The obtained liquid was then subjected to vacuum evaporation for dichloromethane removal and stored in desiccator before characterization. The same procedure was applied for the synthesis of MnTPP crystals. The precipitation of MnTPP crystals from the synthesis mixture i.e., DMF, requires the solution mixture be mixed with the chilled NaCl solution. The molecular structures for both the synthesized materials are presented in

Fig. 2.

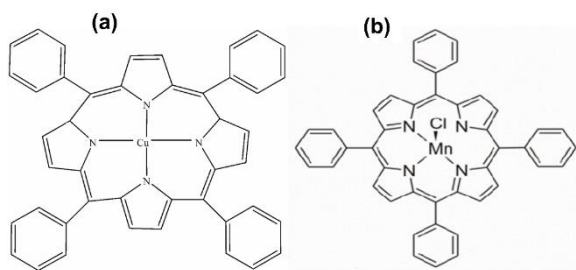


Fig. 2: Structure of (a) CuTPP [17] (b) MnTPP [18].

Characterization

CHN Analysis

The analytical and stoichiometry for C, H and N determination as provided in

Table-1 revealed similar values which agree well with the literature [19].

Table-1: C, H and N analysis of the MePs.

Method	C (%)	H (%)	N (%)
CuTPP (Analytical)	85.96	5.63	8.4
MnTPP (Analytical)	85.39	5.19	9.4
Calculated	86.27	4.57	9.15

XRD Results

For the CuTpp the XRD analysis performed between (5°-60°), and is presented in

Fig. 3(a), The pattern matched well with the PAN-ICSD (Panalytical-Internationals crystal structure database) reference code 00-054-1330 [20].

For CuTPP a bravais type primitive (P) Tetragonal crystal system was found, with unit cell parameters a: 8.617 Å, b: 8.617 Å and c: 20.55 Å with Alpha, Beta and Gamma being 90° respectively. Density was calculated to be 1.31 g.cm⁻³ with cell volume 1525.83 Å³. The obtained results are in line with the literature values [21, 22].

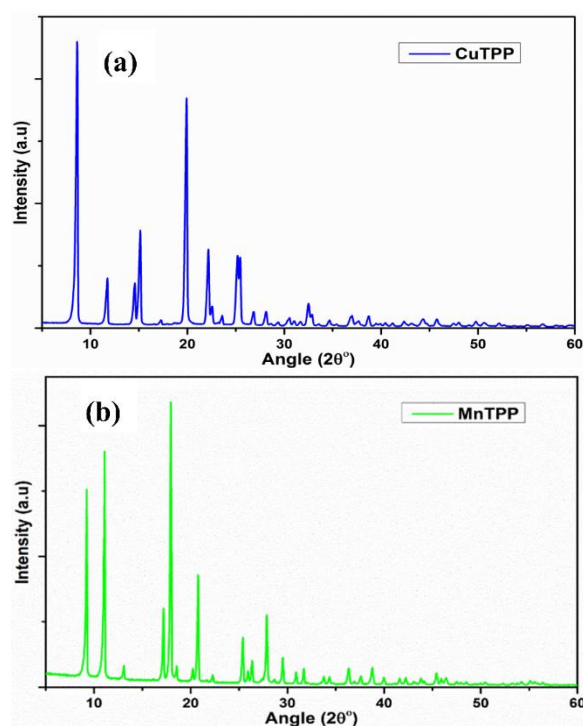


Fig. 3: XRD pattern of synthesized samples (a) CuTPP (b) MnTPP.

The crystal system for MnTPP XRD pattern as given in

Fig. 3(b) with COD (crystallographic open database) reference code 96-200-4472 [23] was Tetragonal having space group number 87 and space group allocation of I 4/m. The unit cell parameters a, b and c were 13.4630 Å, 13.4630 Å and 9.8640 Å respectively, and α , β and γ being 90° respectively. The cell volume 1787.87 Å³ with density 1.31 g.cm⁻³. The results match with that reported by Zhang et al [24].

FTIR Analysis

The FTIR analysis of the synthesized MnTPP and CuTPP is provided in

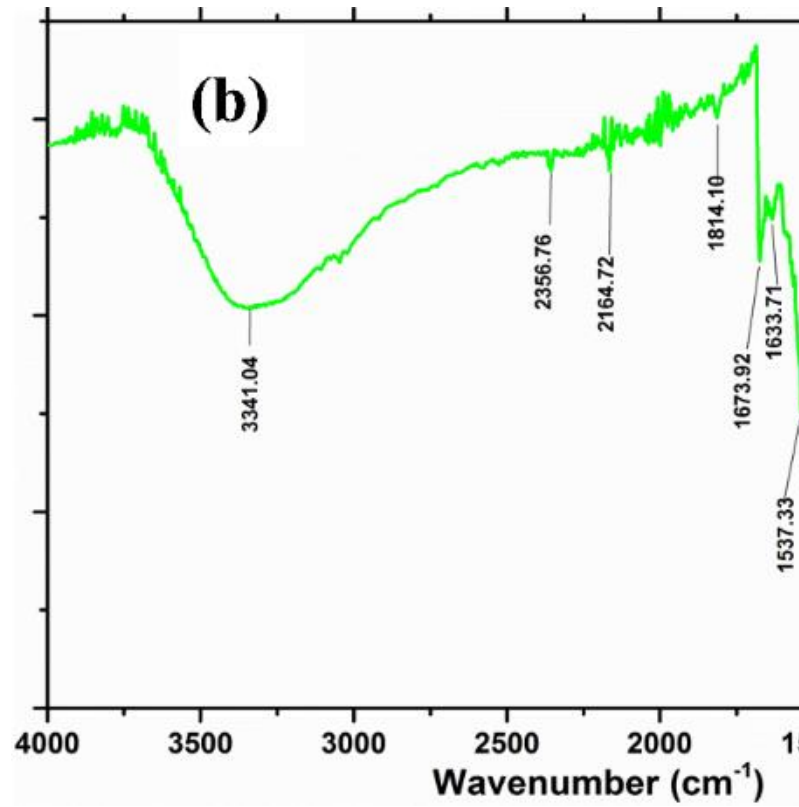
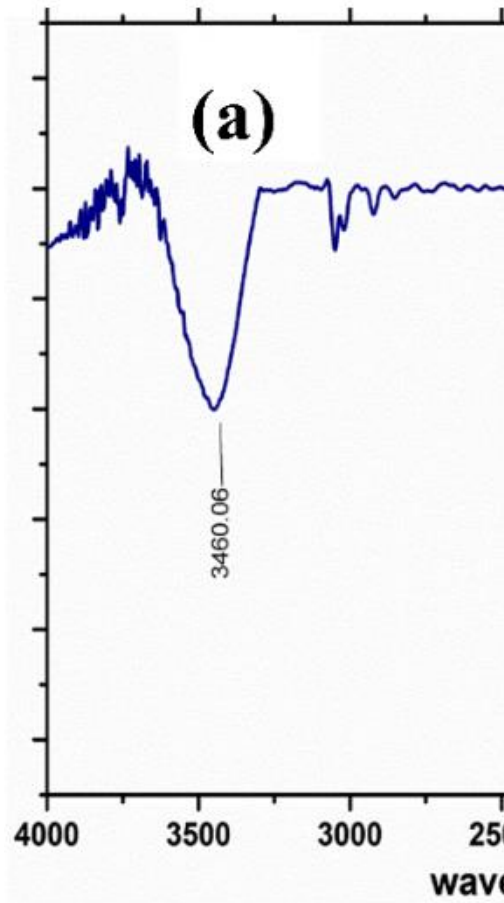


Fig. 4(a) and

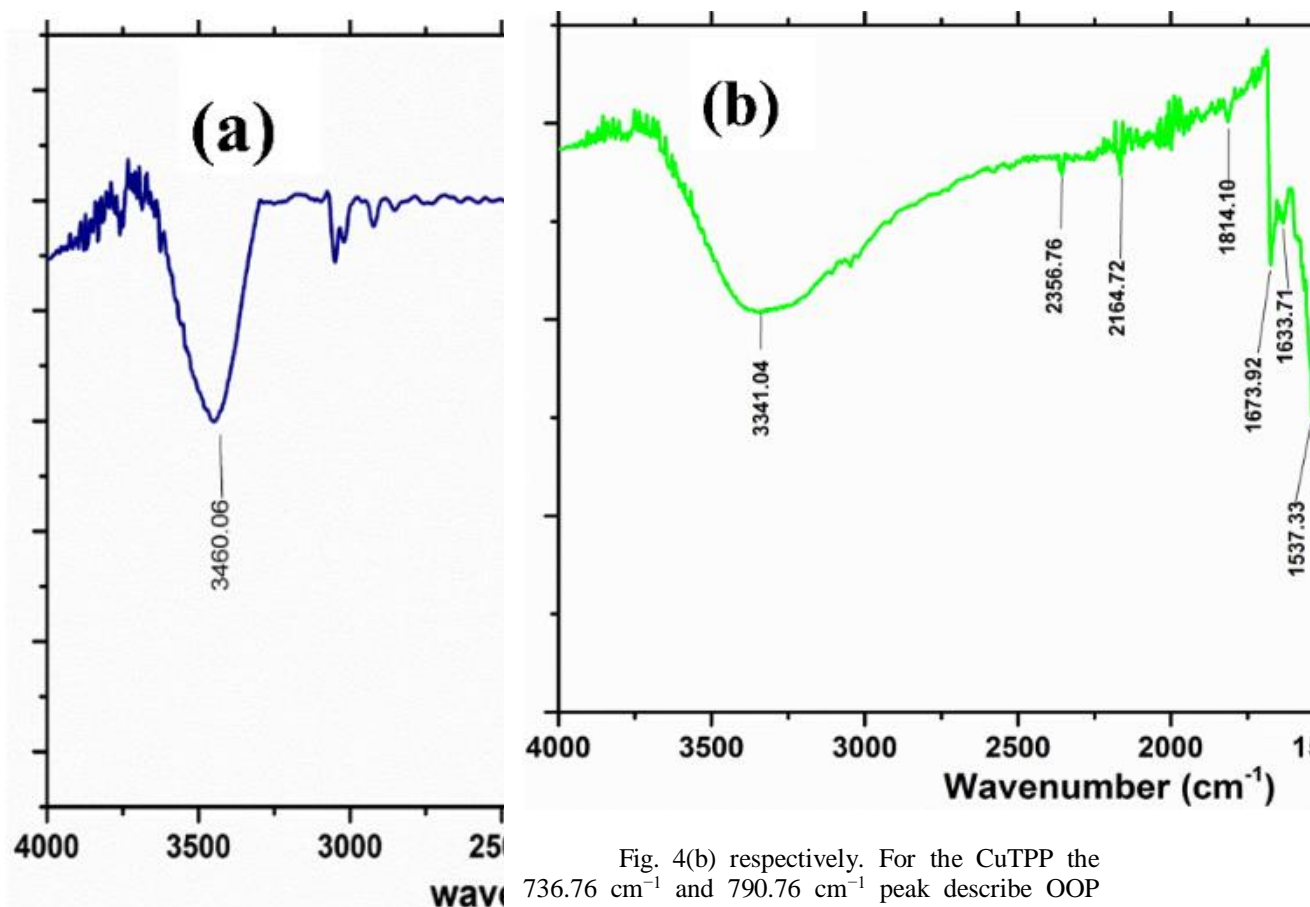


Fig. 4(b) respectively. For the CuTPP the 736.76 cm^{-1} and 790.76 cm^{-1} peak describe OOP bending of the meso-substituted phenyl rings. The peak at 833.19 cm^{-1} owes to in-plane distortion of the pyrrole ring. the 999.06 cm^{-1} peak gives pyrrole ring breathing mode, confirming CuTPP formation. The 1066.56 cm^{-1} peak dictates C--C and C--N bond stretching vibrations. The 1342–1398 cm^{-1} peak provides vibrational stretching of the half and quarter-ring as portrayed by the peak at 1340.43 cm^{-1} . The spectral regions 1432–1536 cm^{-1} contain some closely spaced bands. The 1487.01 cm^{-1} and 1593.09 cm^{-1} peaks are ascribed to asymmetric C--C bond vibrational stretching of phenyl rings. The peaks at 1432–1441 cm^{-1} , 1484–1507 and 1572–1576 might be attributed to the C--C bond stretching vibration. The 1631.67 cm^{-1} and 1662.52 cm^{-1} peaks are ascribed to the asymmetric C=C vibrational stretching. The 3460.06 cm^{-1} peak might be attributed to weak -OH stretching owing to the existence of coordinated water adherence over the surface while storage and further dispensation [21, 25-28].

For the MnTPP as given in the the

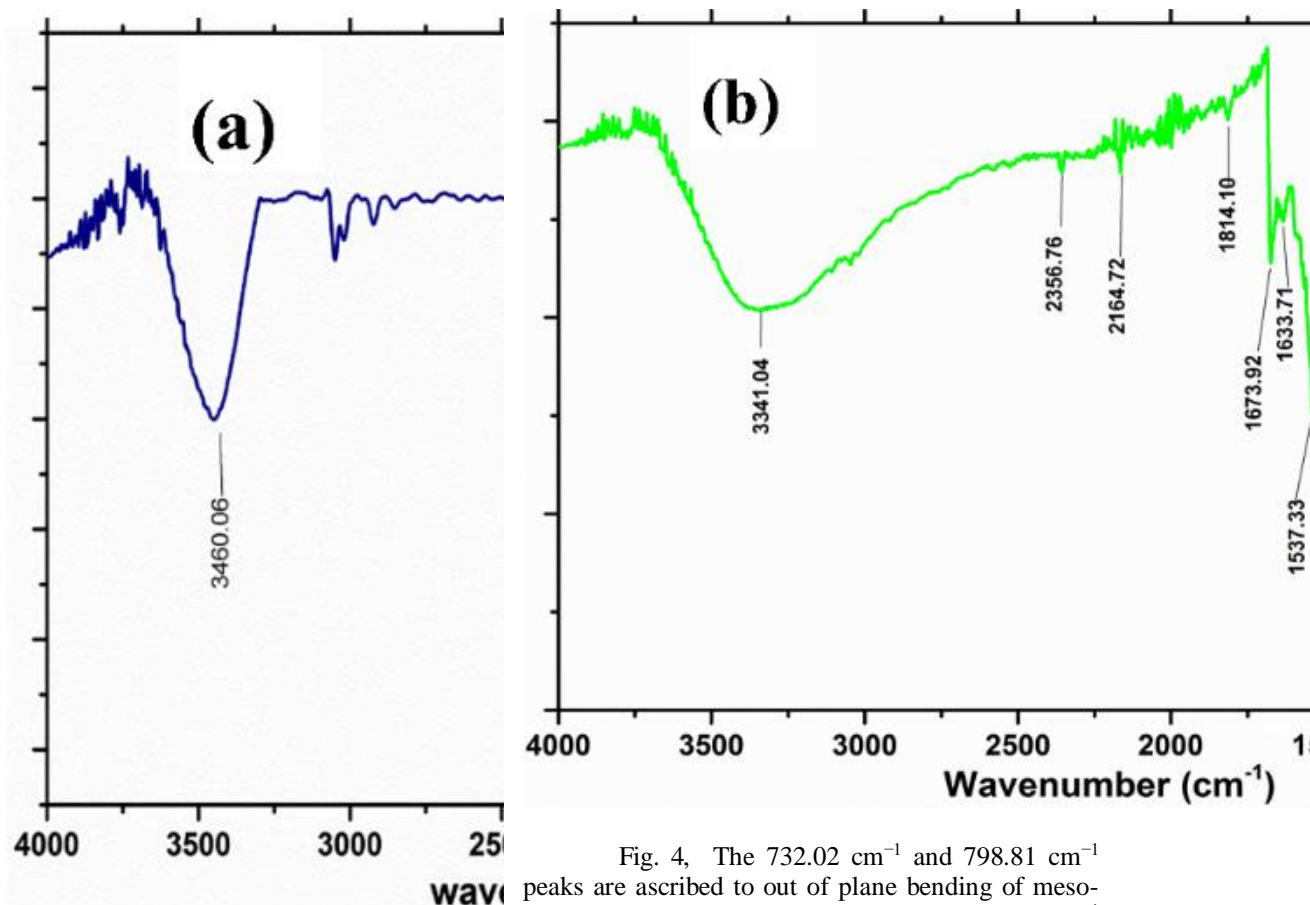
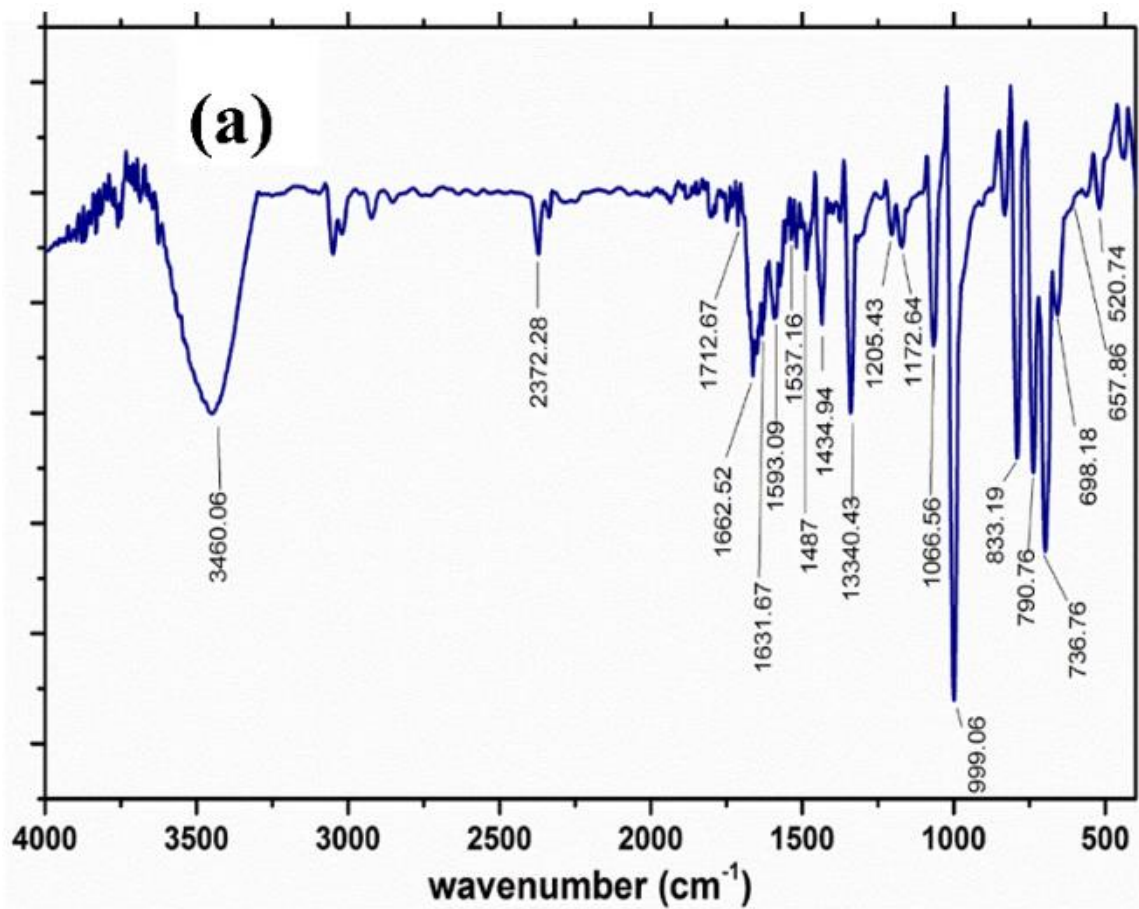


Fig. 4, The 732.02 cm^{-1} and 798.81 cm^{-1} peaks are ascribed to out of plane bending of meso-substituted phenyl rings. The peak at 850.25 cm^{-1} describes pyrrole ring in-plane distortion. The 1009.51 cm^{-1} peak is ascribed to the pyrrole ring breathing mode confirming MnTPP formation. The signal at 1071.89 cm^{-1} provides C--N and C--C bonds stretching vibrations. The $1342\text{--}1398\text{ cm}^{-1}$ peaks advise vibrational stretching of the half and quarter-ring as evident from 1343 cm^{-1} peak. The $1432\text{--}1538\text{ cm}^{-1}$ region contain several closely spaced bands. The 1485.37 cm^{-1} and 1537.33 cm^{-1} peaks are attributed to the asymmetric C--C bond vibrational stretching of the of the phenyl rings. The $1432\text{--}1441\text{ cm}^{-1}$, $1484\text{--}1507$ and $1572\text{--}1576$ peaks are acknowledged as the C--C bond stretching vibration. The asymmetric C=C vibrational mode stretching can be ascribed to the peaks at 1633.71 cm^{-1} and 1673.92 cm^{-1} . The 3341.04 cm^{-1} peak may be credited to the -OH stretching due to the presence of coordinated water molecules attached to the surface during storage and further processing [28-31].



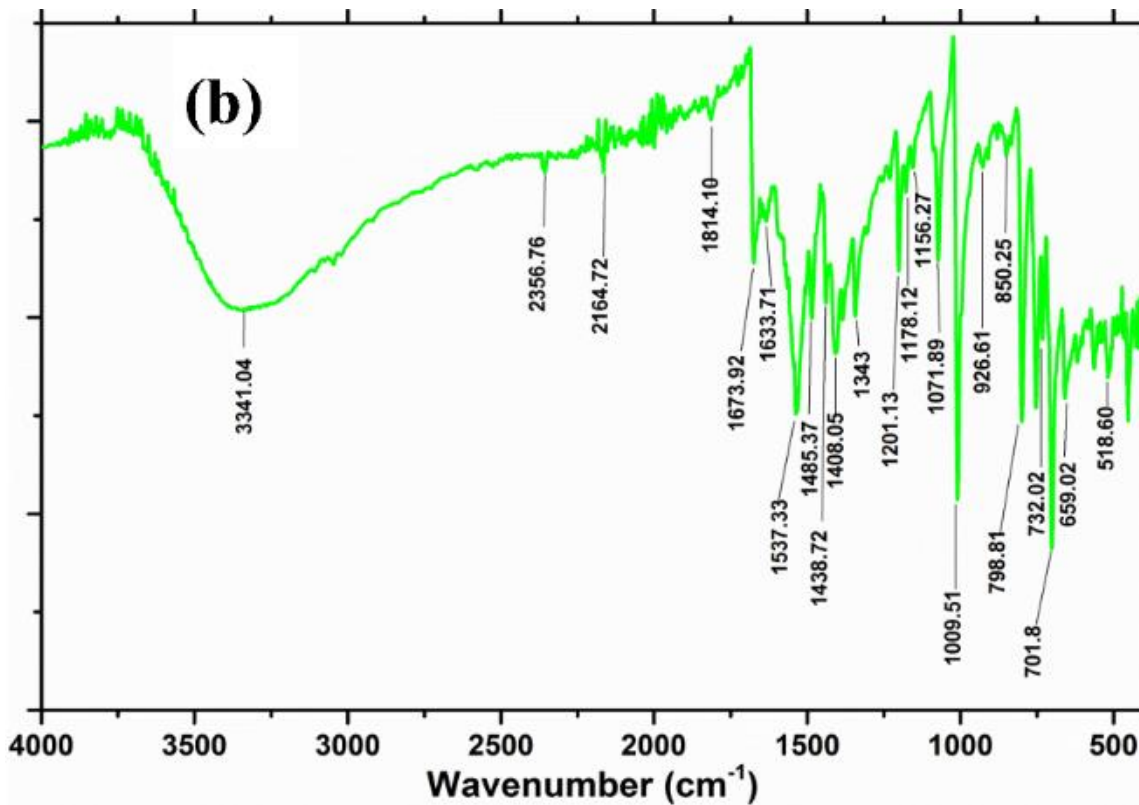


Fig. 4: FTIR spectrum of the synthesized metalloporphyrin (a) CuTPP [16] (b) MnTPP.

TGA Analysis

The thermogravimetric analysis (TGA) of both CuTPP and MnTPP is presented in

Fig. 5 where it can be seen that the initial weight loss for both the samples follows the same route until 130°C and then a weight loss can be observed till 200°C which is attributed to the presence of water in the samples. At 400°C second weight loss is observed for both samples and is approximately 50 weight % for CuTPP up till 550°C and for MnTPP the second weight loss is 70 weight % up till 800°C.

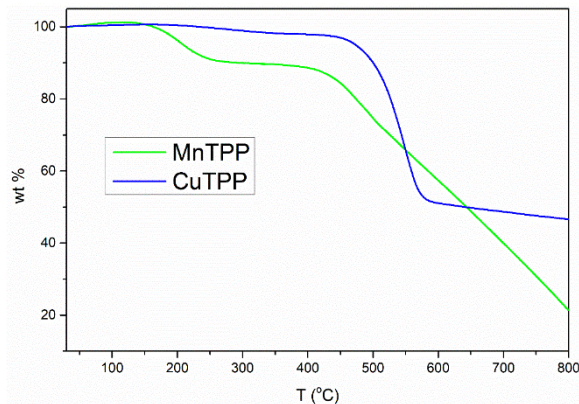


Fig. 5: TGA analysis of CuTPP and MnTPP.

UV-Vis Results

Peaks in the range of 250-600 in the UV-vis spectrum displayed in

Fig. Error! No text of specified style in document.6 indicate conjugated molecules presence. The solet (S) band at 418 nm, indicates the existence of the metalloporphyrin moiety in the synthesized material, with 538 nm and 620 nm Q bands displaying significant absorbance to confirm metalation of the free base porphyrin [32].

MnTPP's Q bands found at 515 nm, 550 nm, 589 nm, and 646 nm. The UV-Visible analysis confirms the XRD and FTIR results by revealing the production of the target molecule. The findings are nearly identical to those reported by Zheng et al. [33].

Optimization of Temperature and time for CuTPP and MnTPP synthesis

Table-2 shows that CuTPP and MnTPP yields are directly proportional to reaction temperature (T) and residence time (t) [34]. This is because at higher temperatures, bond energies excite and increase conversion with time.

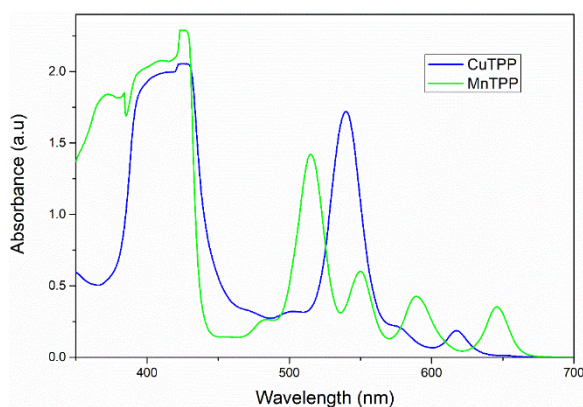
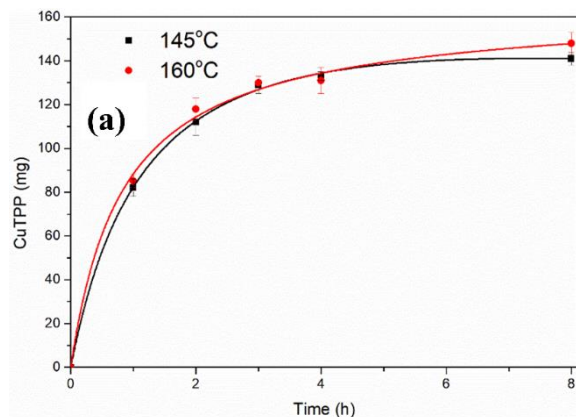


Fig. Error! No text of specified style in document.6: UV-visible spectra of CuTPP and MnTPP in Dichloromethane.



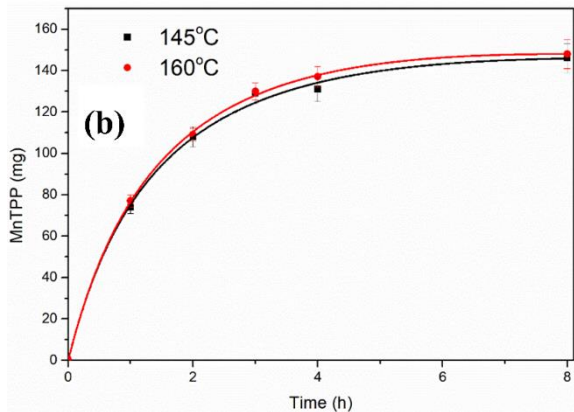


Fig 7 (a) shows the experimental results of CuTPP and

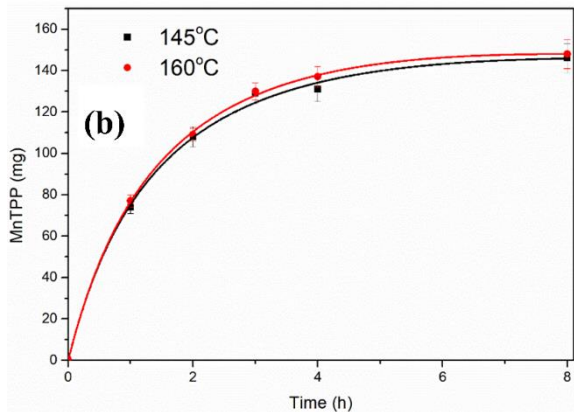
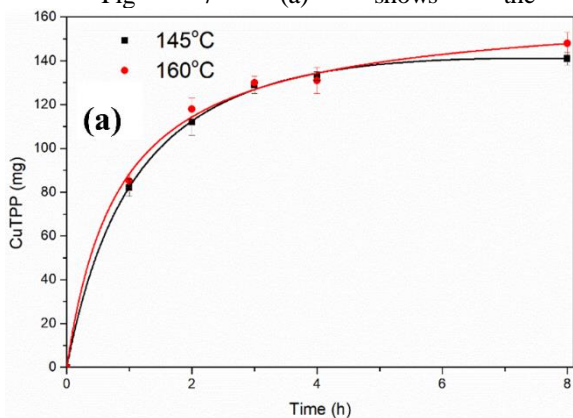


Fig 7 (b) for MnTPP yields at different reaction temperatures (145°C and 160°C) against time. It may be noted that too much increase in the residence time or temperature will not be feasible, since it will require a lot of energy to achieve it. Therefore, an optimum set of values is sought which will enhance the yield without significant energy requirements.

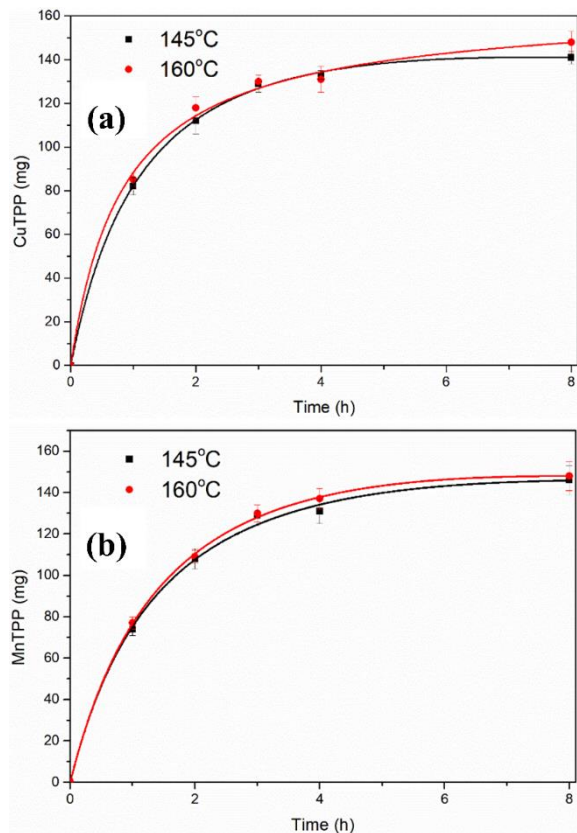


Fig 7: Yields of (a) CuTPP and (b) MnTPP at different reaction temperatures and residence times with fitted curves.

Table-2: CuTPP and MnTPP yield in (mg) w.r.t time (h).

Time (h)	CuTPP (mg)		MnTPP (mg)	
	145°C	160°C	145°C	160°C
0	0	0	0	0
1	82±4	85±3	74±3	77±3
2	112±6	118±5	108±5	109±3
3	129±4	130±3	129±5	130±4
4	133±2	131±6	131±6	137±5
8	141±3	148±5	146±7	148±7

Nelder equation [35] was used to correlate the yield as a function of reaction temperature and residence time, which is applied to account for the temperature rate effect and modelling [36]. The following equation is formed:

$$Y = \frac{t+a}{b_0+b_1(t+a)+b_2(t+a)^2} \tag{1}$$

where,

Y = Yield of MeP (mg), b_i = coefficients (Function of Temperature), t = time (h), a = time shifting factor.

The coefficients b_i in Equation 1 are linear function of temperature [37]. Table-3 presents the correlation parameters for the estimation of CuTPP and MnTPP yields as a function of residence time (t). It can be noted that the shift parameter a is zero, which means that the best fits are achieved without shifting the residence time. The coefficient of determination R^2 and mean absolute percentage deviation (MAPD) for this correlation are 99.99% and 0.73% respectively.

Table-3: Prediction Parameters for MeP yield at various residence times.

Parameters	CuTPP		MnTPP	
	145°C	160°C	145°C	160°C
<i>a</i>	0	0	0	0
<i>b₀</i>	6.76×10 ⁻³	5.1×10 ⁻³	8.2×10 ⁻³	8.25×10 ⁻³
<i>b₁</i>	5.26×10 ⁻³	6.21×10 ⁻³	4.97×10 ⁻³	4.66×10 ⁻³
<i>b₂</i>	1.24×10 ⁻⁴	-9.84×10 ⁻⁶	1.07×10 ⁻⁴	1.33×10 ⁻⁴

The parameters ‘a’ and ‘c’ determined for the correlation are assumed to be linear functions of temperature. This means that:

$$b_i = c_i T + d_i \quad , \quad 0 \leq i \leq 2 \quad (2)$$

Since a = 0, the resulting Equation (4.1) now reduces to

$$Y_{(T,t)} = \frac{t}{(c_0 T + d_0) + (c_1 T + d_1)t + (c_2 T + d_2)t^2} \quad (3)$$

Resulting in the overall Yield prediction parameter to be

$$Y_{(T,t)} = \frac{t}{(c_0 + c_1 t + c_2 t^2)T + (d_0 + d_1 t + d_2 t^2)} \quad (4)$$

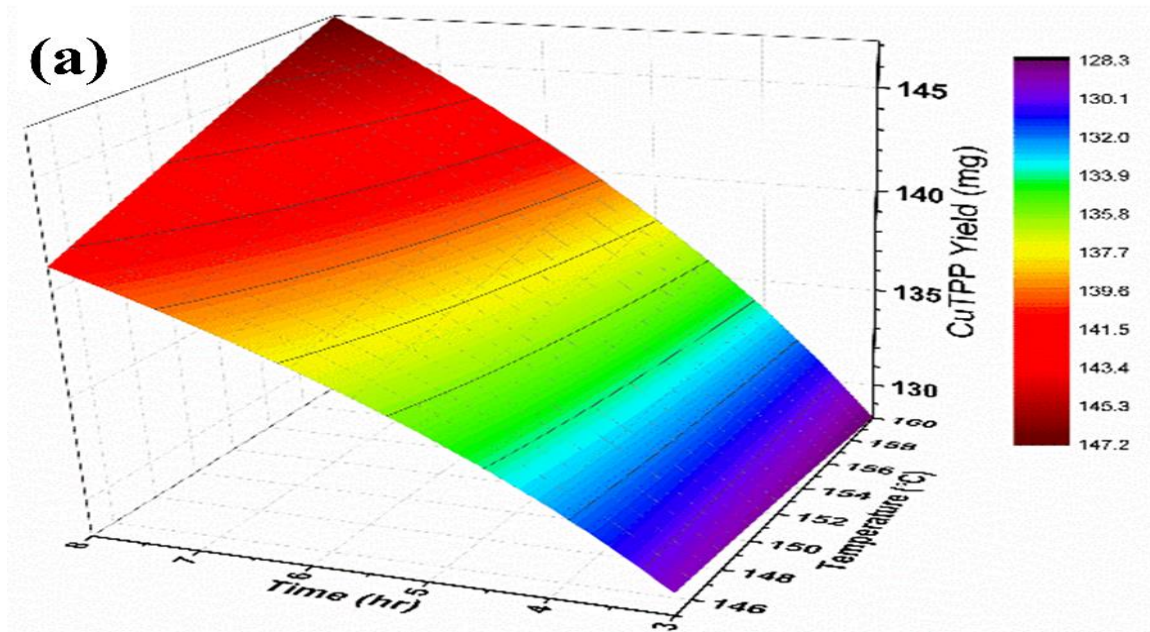
Fig. 8 (a), and

Fig. 9(a), show the surface plots, whereas

Fig. 8 (b) and

Fig. 9 (b), show the contour plots for CuTPP and MnTPP yield predictions respectively. It is observed that the yield is directly proportional to both the reaction temperature (T) and the residence time (t). Since the yield correlations are accurately predicting the experimental observations, they may be utilized for yield predictions within the identified ranges of residence time (t ≤ 8 h) and reaction temperature (145°C ≤ T ≤ 160°C).

Table-4, presents the prediction parameters that to maintain it throughout the reaction were used. To determine the energy supplies for all setups, the energy needed to attain the reaction temperature and approximated as in Equation 5.



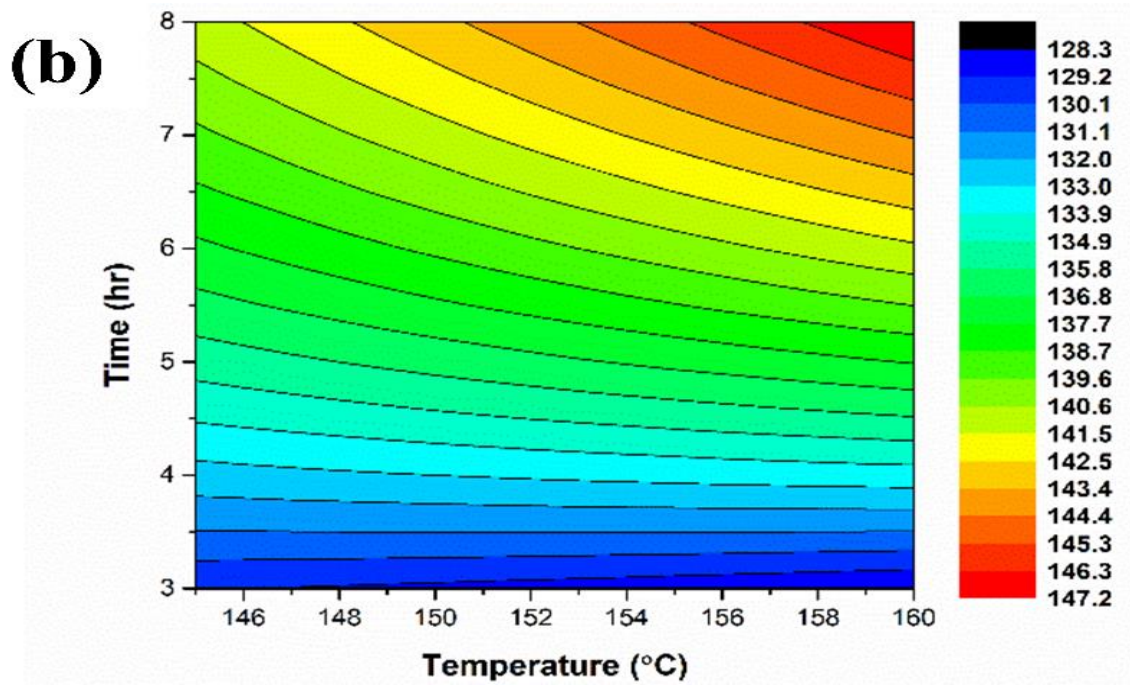
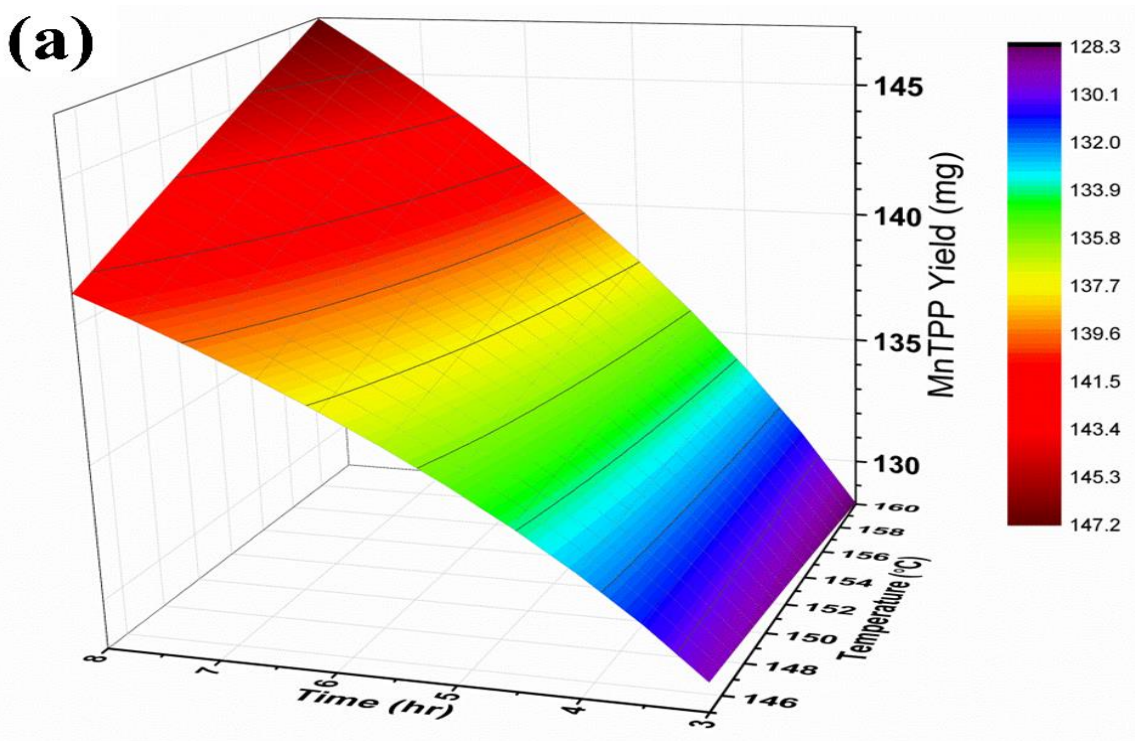


Fig. 8: CuTPP yield predictions (a) Surface plot (b) Contour plot.



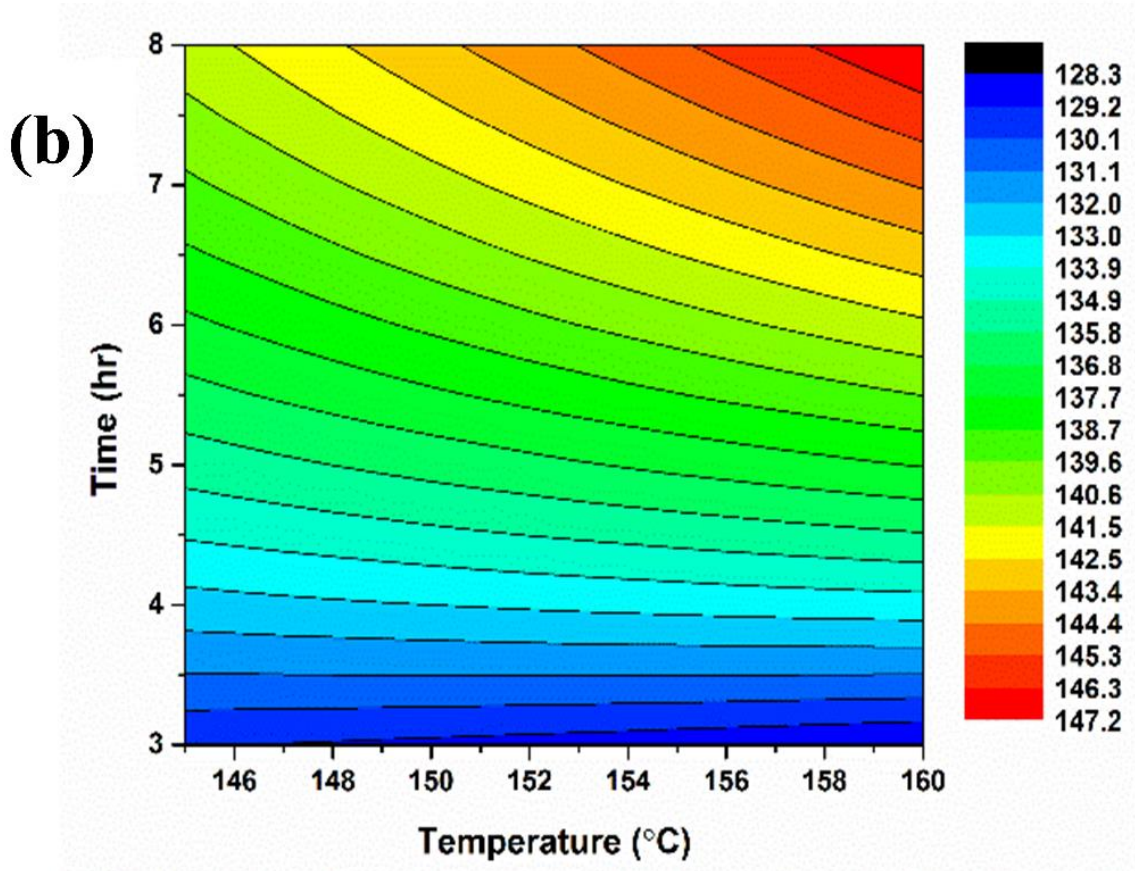


Fig. 9: MnTPP yield predictions (a) Surface plot (b) Contour plot.

Table-4: Yield correlations of CuTPP and MnTPP – Prediction Parameters.

Parameters	CuTPP	MnTPP
c_0	-1.11×10^{-4}	3.33×10^{-6}
c_1	6.33×10^{-5}	-2.07×10^{-5}
c_2	-8.90×10^{-6}	1.72×10^{-6}
d_0	2.28×10^{-2}	7.72×10^{-3}
d_1	-3.92×10^{-3}	7.97×10^{-3}
d_2	1.41×10^{-3}	-1.42×10^{-4}

$= 0.0373 \text{ kJ/min}$

Energy $\alpha f(\text{Temperature}) + f(\text{Time})$

$E = f(T) + f(t)$

Temperature to reach 145°C required 45±10 min

Temperature to reach 160°C required 60±10 min

Therefore,

for 145°C, $E = 0.0373 \times 45 \text{ min}$

for 160°C, $E = 0.0373 \times 60 \text{ min}$

This can be combined as

$E = 0.0373(T-100)$

Since

$145 - 100 = 45$

The energy utilization plot (in kJ) shown in Fig. 10 is dependent on residence time and maintained temperature. It can be noted that higher reaction temperatures or residence times require more energy. The derivation of Equation 5 is given below.

The energy was supplied through Hot Plate with magnetic stirring and the chiller for the reflux condenser water.

Chiller energy input = 1210 W

Hot Plate energy input = 1030 W

Total energy input = 2240 W or 2.240 kJ/s or 2.240 kJ/s × 60 s/min

$$160 - 100 = 60$$

Therefore

$$E = 0.0373 (T - 100 + 60 t)$$

Therefore, the equation is,

$$E_{(T,t)} = 0.0373 (T - 100 + 60t) \quad (5)$$

It can be inferred that a higher product yield will require more residence time and temperature [34]. However, the providence of high temperature as well as high residence time may be uneconomical, as it demands a higher energy input. Therefore, finding the optimum formation is useful to maximize productivity (P), which means obtaining sufficient product without requiring too much energy.

The optimization problem is solved as follows:

$$\text{Max } P_{(T,t)} \quad (6)$$

Subject to:

$$P_{(T,t)} = Y_{(T,t)} - E_{(T,t)} \quad (7)$$

$$Y_{(T,t)} = \frac{t}{(c_0 + c_1 t + c_2 t^2)T + (d_0 + d_1 t + d_2 t^2)} \quad (4)$$

$$E_{(T,t)} = 0.0373 (T - 100 + 60t) \quad (5)$$

$$145 \leq T \leq 160, 0 \leq t \leq 8, 0 \leq Y, 0 \leq E$$

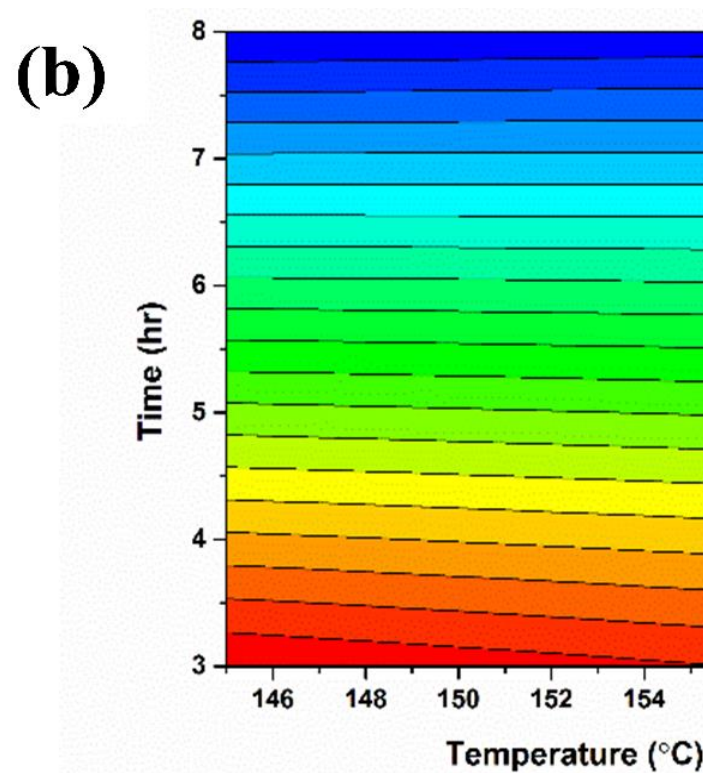
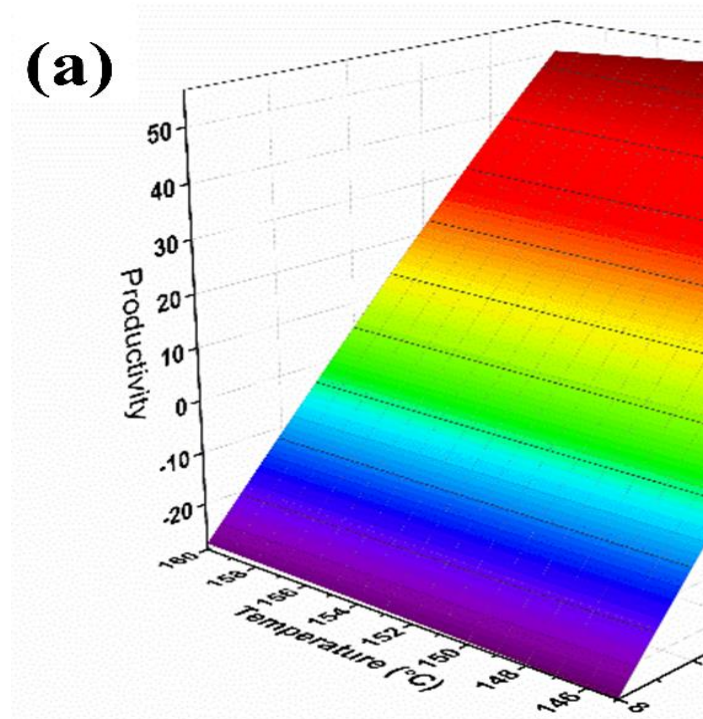


Fig. 11 and Fig. 12 present the surface and contour projections of the objective function plotted through

MATLAB. It can be observed from 145 °C till 160 °C. The contour plot in

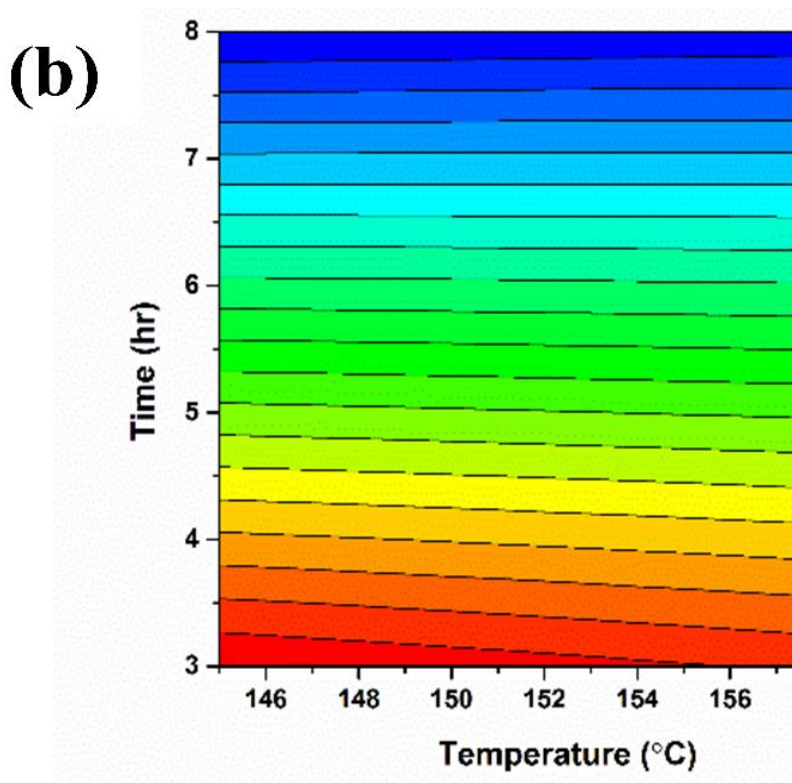
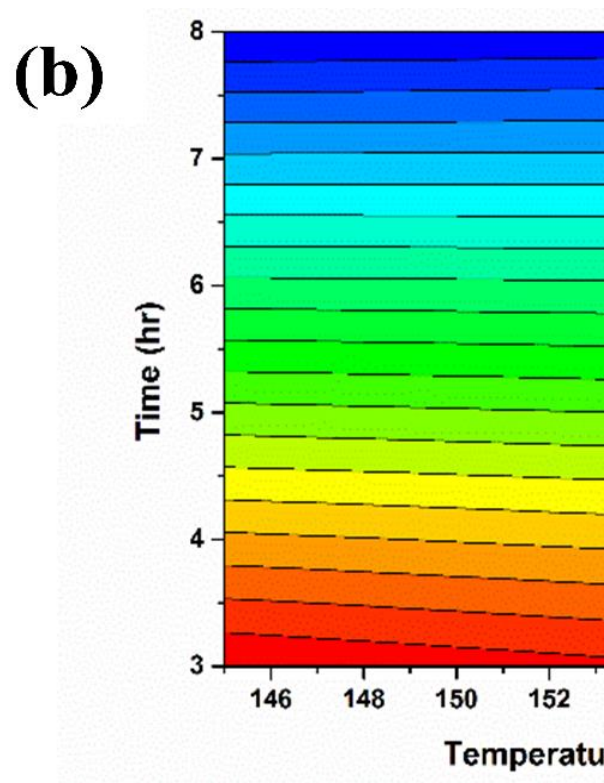
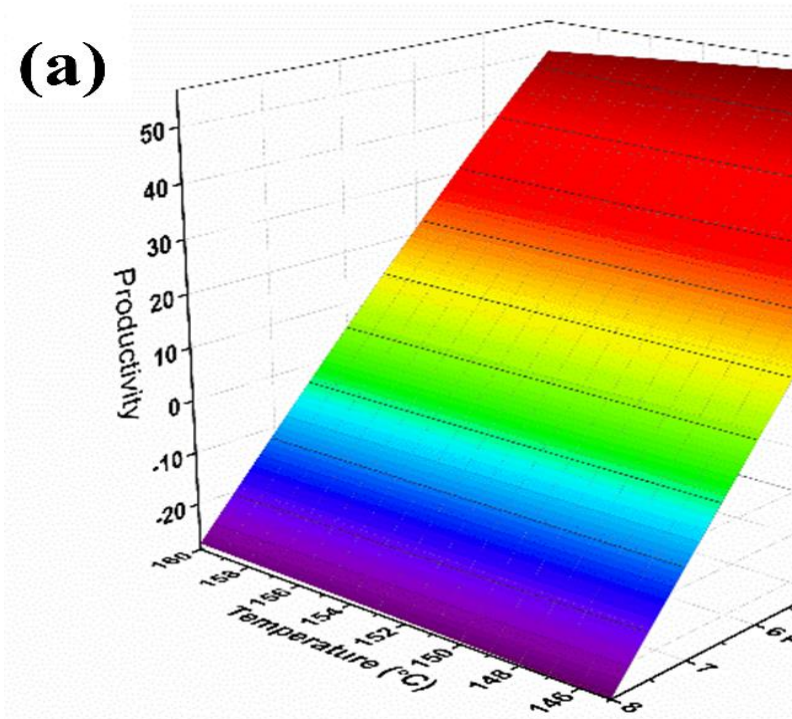
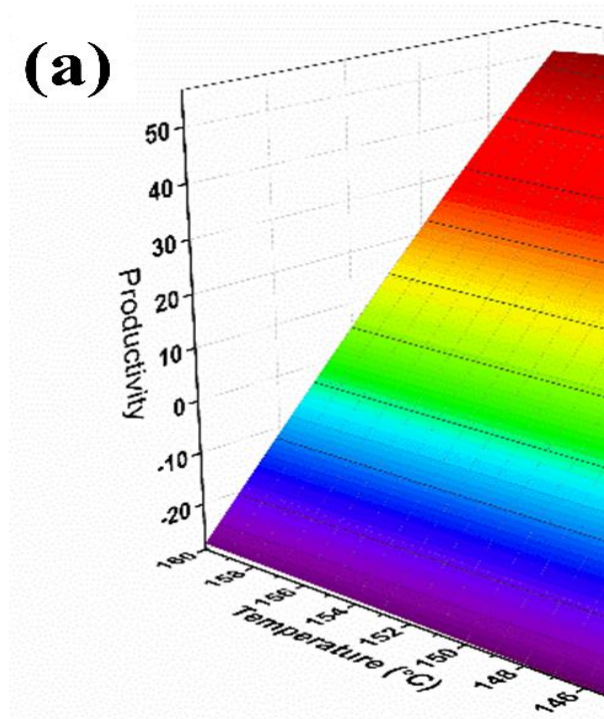


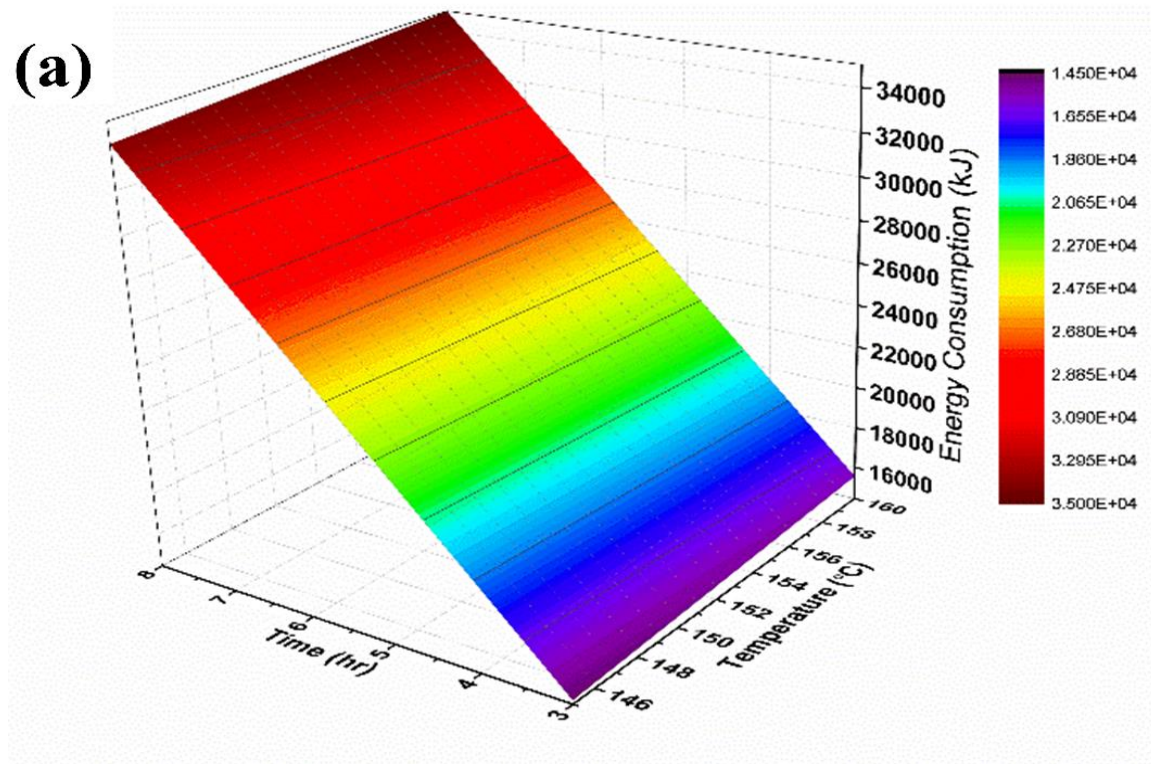
Fig. 11(a) that the objective function (productivity) is decreasing from 3 h to 8 h and from

Fig. 11 (b) gives a uniform value distribution of the productivity from 8 h till 7.34 h

and then start converging towards 3 h and 145 °C. The same phenomenon can be observed with MnTPP in

Fig. 12(a) that the objective function (productivity) is decreasing from 3 h to 8 h and from 145 °C till 160 °C. The contour plot in

Fig. 12(b) gives a uniform value distribution of the productivity from 8 h till 5.89 h and then start converging towards 3 h and 145 °C.



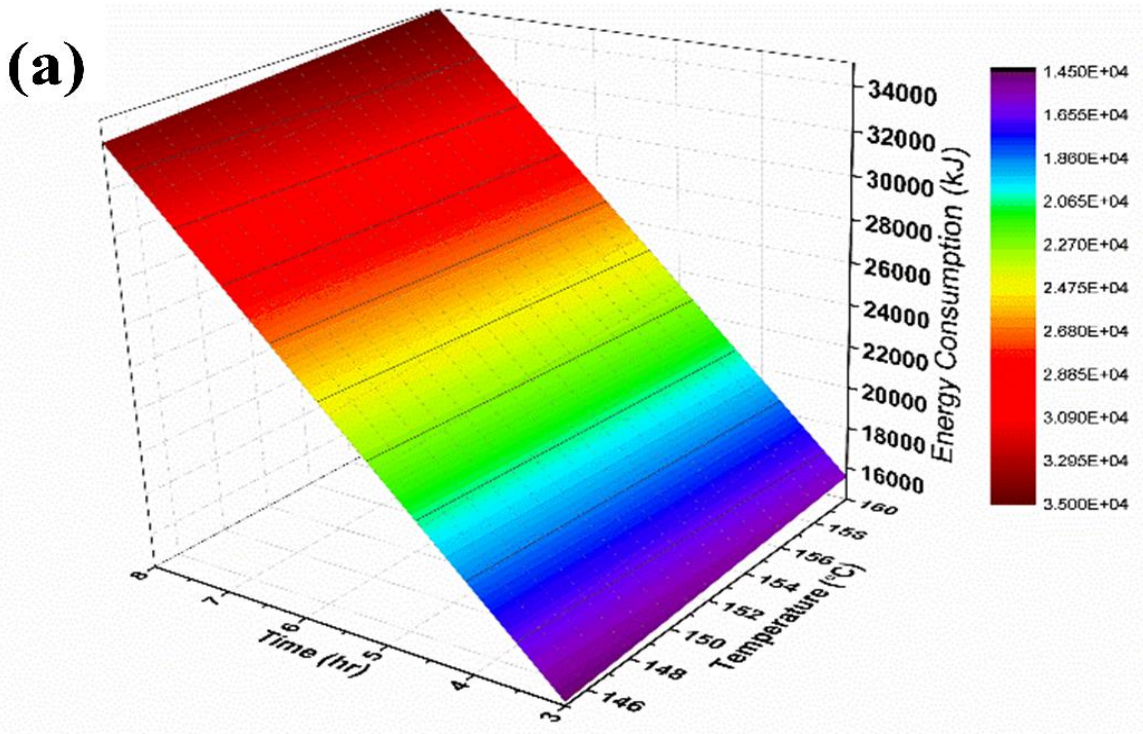
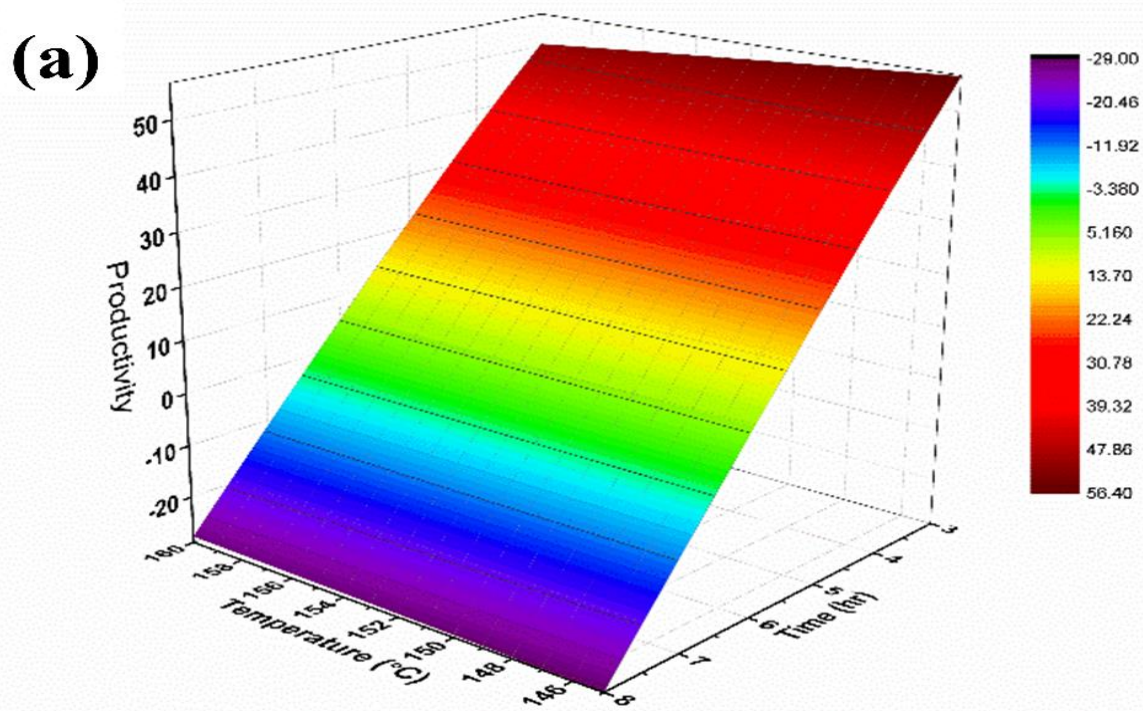


Fig. 10: (a) Energy demand for reaction(s) (b) Contour plot of the function.



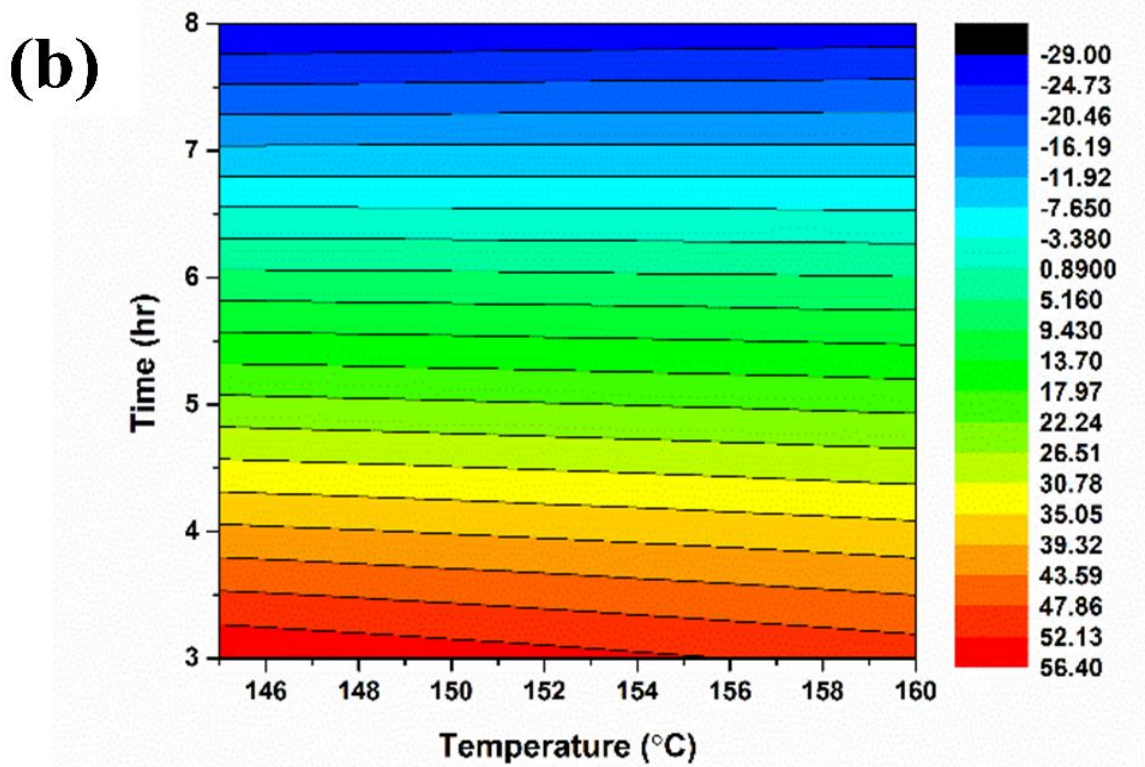
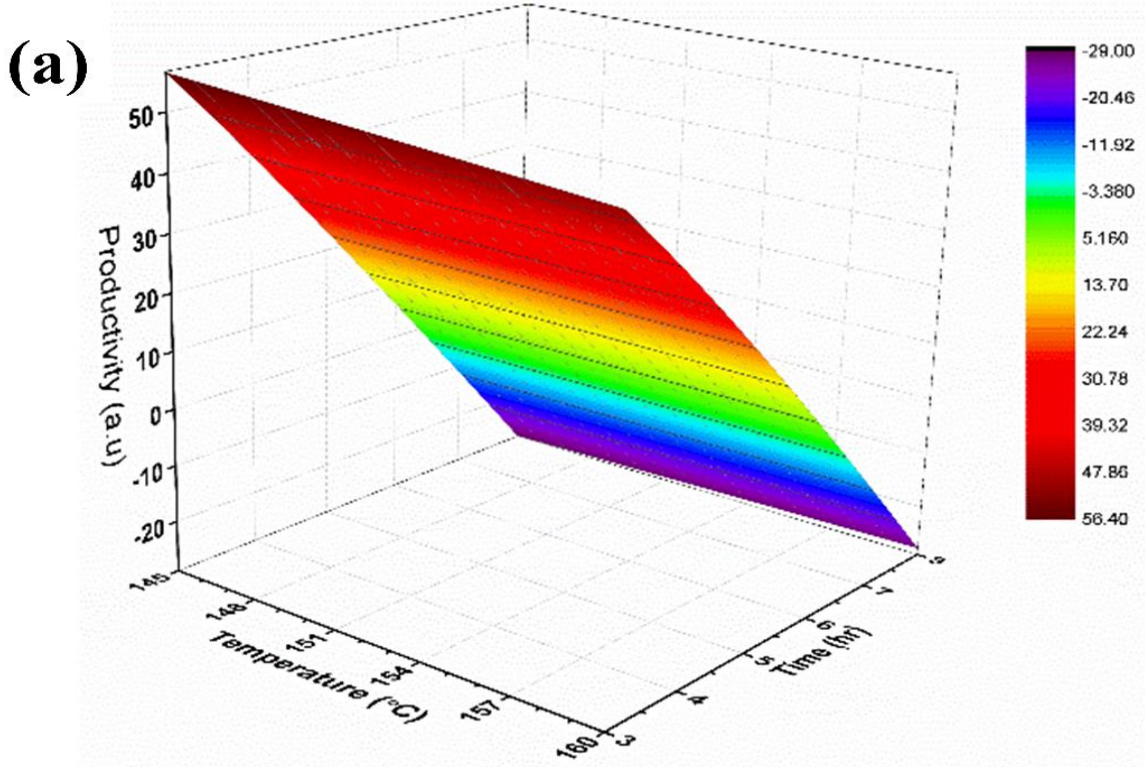


Fig. 11: (a) Surface and (b) Contour plot of the CuTPP productivity function.



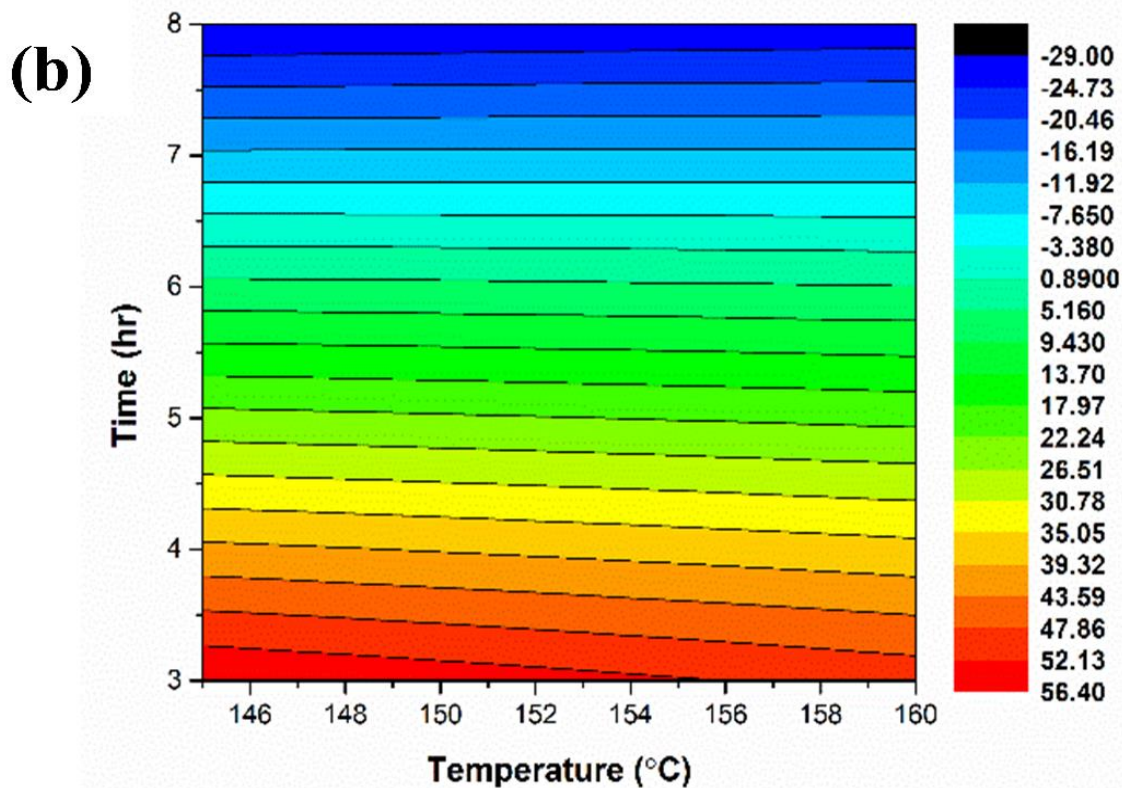


Fig. 12: (a) Surface and (b) Contour plot of the MnTPP productivity function.

Conclusion

One-pot synthesized dark purple CuTPP and dark green MnTPP crystals were characterized to confirm the presence of target macrocyclic ligand and for their physicochemical characteristics. From the CHN analysis, it was observed that the MePs atomic composition of elements are consistent with the stoichiometric calculations. Further confirmation of the synthesis of target molecules was obtained from XRD analysis, as the exact match of the crystallographic patterns from the ICDD and COD database was found. TGA analysis further confirmed the CHN results. The required functional groups were present as confirmed via FTIR spectrum. The synthesized ligands were then studied for optimization by varying time and temperature minimizing the energy input as the objective function. The optimized values for the residence time and temperature with respect to the energy consumption were evaluated for the synthesis of CuTPPs and MnTPPs using MATLAB for which the calculated parameters came out to be 3.7 hrs and 145°C respectively.

Reference

1. K. M. Kadish, K. M. Smith and R. Guilard, Ed.^Eds. The Porphyrin Handbook: Inorganic, organometallic and coordination chemistry, ed. (no.). Elsevier, 2000, p.^pp.
2. K. S. Suslick, N. A. Rakow, M. E. Kosal and J.-H. Chou, The materials chemistry of porphyrins and metalloporphyrins, *Journal of Porphyrins and Phthalocyanines*, 4, 4, (2000).
3. S. Nakagaki, G. K. B. Ferreira, G. M. Ucoski and K. A. Dias de Freitas Castro, Chemical reactions catalyzed by metalloporphyrin-based metal-organic frameworks, *Molecules*, 18, 6, (2013).
4. T. Aida and S. Inoue, Metalloporphyrins as initiators for living and immortal polymerizations, *Accounts of chemical research*, 29, 1, (1996).
5. V. Bulach, F. Sguerra and M. W. Hosseini, Porphyrin lanthanide complexes for NIR emission, *Coordination Chemistry Reviews*, 256, 15, (2012).
6. R. Chouikrat, A. Champion, R. Vanderesse, C. Frochet and A. Moussaron, Microwave-assisted synthesis of zinc 5-(4-carboxyphenyl)-10, 15, 20-triphenylporphyrin and zinc 5-(4-

- carboxyphenyl)-10, 15, 20-triphenylchlorin, *Journal of Porphyrins and Phthalocyanines*, 19, 04, (2015).
7. K. Ladomenou, M. Natali, E. Iengo, G. Charalampidis, F. Scandola and A. G. Coutsolelos, Photochemical hydrogen generation with porphyrin-based systems, *Coordination Chemistry Reviews*, 304, (2015).
 8. A. Tiwari and U. Pal, Effect of donor-donor- π -acceptor architecture of triphenylamine-based organic sensitizers over TiO_2 photocatalysts for visible-light-driven hydrogen production, *International Journal of Hydrogen Energy*, 40, 30, (2015).
 9. R. Giovannetti, The use of Spectrophotometry UV-Vis for the Study of Porphyrins, Edited by Jamal Uddin, 87, (2012).
 10. A. Kumar, S. Maji, P. Dubey, G. J. Abhilash, S. Pandey and S. Sarkar, One-pot general synthesis of metalloporphyrins, *Tetrahedron Letters*, 48, 41, (2007).
 11. S. Nadeem, A. Mumtaz, M. S. Alnarabiji, M. I. A. Mutalib and B. Abdullah, Highly porous Zr-MCM-48 immobilized Cu-porphyrin for photocatalytic reduction of CO_2 to methanol in a slurry reactor, *Journal of Materials Science: Materials in Electronics*, 32, 17, (2021).
 12. M. Haas, S. Gonglach and W. Schöfberger, Meso-alkynyl corroles and their cobalt(III), manganese(III) and gallium(III) complexes, *Journal of Porphyrins and Phthalocyanines*, 24, 05n07, (2020).
 13. G. Martínez-Edo, M. C. Llinàs, G. Anguera, A. Gibert and D. Sánchez-García, Functionalized mesoporous silica nanoparticles with 2,7,12,17-tetraphenylporphycene, *Journal of Porphyrins and Phthalocyanines*, 24, 01n03, (2020).
 14. K. Sudoh, Y. Satoh, K. Furukawa, H. Nakano and Y. Matano, Synthesis and optical, magnetic, and electrochemical properties of 5,10,15,20-tetraaryl-5,15-diazaporphyrin — tertiary amine conjugates, *Journal of Porphyrins and Phthalocyanines*, 24, 01n03, (2020).
 15. X. Li, K. Li, D. Wang, J. Huang, C. Zhang, Y. Du and P. Yang, One-pot synthesis of manganese porphyrin covalently functionalized graphene oxide for enhanced photocatalytic hydrogen evolution, *Journal of Porphyrins and Phthalocyanines*, 21, 03, (2017).
 16. S. Nadeem, M. I. A. Mutalib and M. Shima, One pot synthesis and characterization of meso-5, 10, 15, 20-copper tetraphenylporphyrin, *RASAYAN Journal of Chemistry*, 9, 3, (2016).
 17. M. M. El-Nahass, A. M. Hassanien, F. S. H. Abu-Samaha and E. Elesh, Effect of illumination on the structural and optical properties of Cu (II) tetraphenyl porphyrin (CuTPP) thin films, *Optics Communications*, 325, Supplement C, (2014).
 18. J. P. Beggan, S. A. Krasnikov, N. N. Sergeeva, M. O. Senge and A. A. Cafolla, Control of the axial coordination of a surface-confined manganese (III) porphyrin complex, *Nanotechnology*, 23, 23, (2012).
 19. A. D. Adler, F. R. Longo, J. D. Finarelli, J. Goldmacher, J. Assour and L. Korsakoff, A simplified synthesis for meso-tetraphenylporphine, *The Journal of Organic Chemistry*, 32, 2, (1967).
 20. G. L. Perlovich, W. Zielenkiewicz, E. Utzig, Z. Kaszkur and O. A. Golubchikov, Thermophysical and structural investigations of crystalline solvates based on tetraphenylporphyrin and its copper complex, *Thermochimica acta*, 279, (1996).
 21. M. El-Nahass, F. Abu-Samaha, S. Menshawy and E. Elesh, Effect of annealing on structural and optical properties of copper tetraphenylporphyrin (CuTPP) thin films, *Optics & Laser Technology*, 64, (2014).
 22. M. El-Nahass, A. Farag, F. Abu-Samaha and E. Elesh, Temperature and frequency dependencies of AC and dielectric characterizations of copper tetraphenyl porphyrin thin films, *Vacuum*, 99, (2014).
 23. B. Cheng and W. R. Scheidt, Chloro (5, 10, 15, 20-tetraphenylporphyrinato) manganese (III) with 4/m Symmetry, *Acta Crystallographica Section C: Crystal Structure Communications*, 52, 2, (1996).
 24. W.-j. Zhang, P.-p. Jiang, P.-b. Zhang and P. Liu, Immobilization of tetraphenylporphyrin manganese (III) chloride in HMS modified by Zr, Cu, and Zn oxides and their catalytic activity, *Catalysis letters*, 142, 12, (2012).
 25. S. S. A. Verma, Metal-tetraphenylporphyrin functionalized carbon nanotube composites as sensor for benzene, toluene and xylene vapors, (2014).
 26. Y. Liu, Y. Yang, Q. Sun, Z. Wang, B. Huang, Y. Dai, X. Qin and X. Zhang, Chemical Adsorption Enhanced CO_2 Capture and Photoreduction over a Copper Porphyrin Based Metal Organic Framework, *ACS applied materials & interfaces*, 5, 15, (2013).
 27. J. Hu, I. Pavel, D. Moigno, M. Wumaier, W. Kiefer, Z. Chen, Y. Ye, Q. Wu, Q. Huang and S. Chen, Fourier-transform Raman and infrared spectroscopic analysis of 2-nitro-tetraphenylporphyrin and metallo-2-nitro-tetraphenylporphyrins, *Spectrochimica Acta Part A: Molecular and Biomolecular Spectroscopy*, 59, 9, (2003).

28. L. J. Boucher and J. J. Katz, The Infrared Spectra of Metalloporphyrins (4000-160 Cm^{-1}), *Journal of the American Chemical Society*, 89, 6, (1967).
29. A. K. Rahiman, K. Rajesh, K. S. Bharathi, S. Sreedaran and V. Narayanan, Manganese (III) porphyrin-encapsulated Ti, Si-mesoporous molecular sieves as heterogeneous catalysts for the epoxidation of alkenes, *Applied Catalysis A: General*, 314, 2, (2006).
30. R. Naik, P. Joshi, S. Umbarkar and R. K. Deshpande, Polystyrene encapsulation of manganese porphyrins: highly efficient catalysts for oxidation of olefins, *Catalysis Communications*, 6, 2, (2005).
31. Z. Li, C.-G. Xia and X.-M. Zhang, Preparation and catalysis of DMY and MCM-41 encapsulated cationic Mn (III)-porphyrin complex, *Journal of Molecular Catalysis A: Chemical*, 185, 1, (2002).
32. E. Fagadar-Cosma, C. Enache, R. Tudose, I. Armeanu, E. Mosoarca, D. Vlasici and O. Costisor, UV-VIS and Fluorescence Spectra of Meso-Tetraphenylporphyrin and Meso-Tetrakis-(4-Methoxyphenyl) Porphyrin in the THF and THF Water Systems The influence of pH, *Revista De Chimie-Bucharest-Original Edition*-, 58, 5, (2007).
33. W. Zheng, N. Shan, L. Yu and X. Wang, UV-visible, fluorescence and EPR properties of porphyrins and metalloporphyrins, *Dyes and Pigments*, 77, 1, (2008).
34. A. V. Bridgwater and D. Boocock, Ed.^Eds. *Developments in Thermochemical Biomass Conversion: Volume 1*, ed. (no.). Springer Science & Business Media, 2013, p.^pp.
35. J. K. A. Bleasdale and J. A. Nelder, Plant Population and Crop Yield, *Nature*, 188, (1960).
36. J. A. Nelder, New Kinds of Systematic Designs for Spacing Experiments, *Biometrics*, 18, 3, (1962).
37. D. A. Ratkowsky, Ed.^Eds. *Handbook of nonlinear regression models*, ed. (no. 04; QA278.2, R3.). 1990, p.^pp.